Clustering of Combined 24-2 and 10-2 Visual Field Grids and Their Relationship With Circumpapillary Retinal Nerve Fiber Layer Thickness

Hideo Nakanishi, Tadamichi Akagi, Kenji Suda, Tomoko Hasegawa, Hiroshi Yamada, Satoshi Yokota, Munemitsu Yoshikawa, Yuto Iida, Hanako Ohashi Ikeda, Satoshi Morooka, Kenji Ishihara, and Nagahisa Yoshimura

Department of Ophthalmology and Visual Sciences, Kyoto University Graduate School of Medicine, Shogoin, Sakyo-ku, Kyoto, Japan

Correspondence: Hideo Nakanishi, Department of Ophthalmology and Visual Sciences, Kyoto University Graduate School of Medicine, 54 Kawaharacho, Shogoin, Sakyo-ku, Kyoto 606-8507, Japan; hideon@kuhp.kyoto-u.ac.jp.

Submitted: December 5, 2015
Accepted: May 17, 2016

Citation: Nakanishi H, Akagi T, Suda K, et al. Clustering of combined 24-2 and 10-2 visual field grids and their relationship with circumpapillary retinal nerve fiber layer thickness. *Invest Ophthalmol Vis Sci*. 2016;57:3203–3210. DOI:10.1167/iovs.15-18798

Purpose. The purpose of this study was to cluster the test points of the combined 24-2 and 10-2 visual fields (VFs) and circumpapillary retinal nerve fiber layer thickness (cpRNFLT) sectors using explanatory factor analyses (EFAs). The correlations between the VF clusters and cpRNFLT clusters were determined, and a new function–structure relationship map was determined.

Methods. Two hundred fifty-four eyes of 166 subjects (13 normal eyes and 241 eyes with glaucoma) were studied retrospectively. All eyes had an axial length <27 mm and had undergone 24-2 and 10-2 VF tests using the Swedish Interactive Threshold Algorithm (SITA-standard) and cpRNFLT examinations by spectral domain optical coherence tomography within a 3-month period. Explanatory factor analysis was performed to group the 116 test points of the combined 24-2/10-2 VF test grids into a smaller number of VF clusters. Another EFA was performed to cluster the 24 cpRNFLT sectors. The correlations between the VF clusters and the cpRNFLT clusters were evaluated by Pearson's correlation analysis.

Results. The combined 24-2/10-2 VF test grids were grouped into seven VF clusters by EFA. Another EFA grouped the cpRNFLT sectors into 11 clusters. The correlation coefficients between the corresponding VF and cpRNFLT clusters ranged from 0.304 ($P < 1 \times 10^{-6}$) to 0.794 ($P < 2.2 \times 10^{-16}$).

Conclusions. Explanatory factor analysis revealed detailed patterns of glaucomatous VF defects and glaucomatous cpRNFL thinning. Their significant correlations indicate that they have common latent factors that might be derived from a developing pattern of glaucomatous optic neuropathy. These findings support the function–structure relationship theory in glaucoma.

Keywords: glaucoma, factor analysis, retinal nerve fiber layer, optical coherence tomography, visual field

Glaucomatous optic neuropathy (GON) usually presents with characteristic visual field (VF) defects caused by a progressive degeneration of the retinal ganglion cells (RGCs) and their axons. Because VF defects are the most important signs of GON, examinations of the VF by standard automated perimetry (SAP), especially using the Swedish Interactive Threshold Algorithm (SITA),[1,2] are the current gold standard for both the diagnosis and management of GON. However, SAP examines many stimulus points; for example, the Humphrey Visual Field Analyzer (HFA; Carl Zeiss Meditec, Dublin, CA, USA) can test a maximum 77 points (76 points in Fig. 1A and 1 point corresponding with the fovea). Short- and long-term fluctuations of the threshold values at each test point are often detected, which hinders an accurate diagnosis by clinicians.[3–5]

Global indices such as the mean deviation (MD) or pattern standard deviation (PSD) values enable a panoramic look at the SAP results, but focal VF changes can be overlooked. To overcome these problems, many earlier investigators proposed grouping the VF test points into clusters.[6–22] By averaging the threshold values within each cluster, clinicians were able to obtain indices that were more sensitive to focal VF changes than global indices and were less affected by fluctuating thresholds of each test point.[10,23]

More recently, the VF test points were clustered to determine the correlations between visual function and retinal structure in glaucomatous eyes.[14–18] Spectral domain optical coherence tomography (SD-OCT) has allowed clinicians to make quantitative evaluations of the retinal nerve fiber layer (RNFL) thickness in a 360° circumpapillary scan, known as the circumpapillary RNFL thickness (cpRNFLT). The cpRNFLT has been used to evaluate the morphologic changes in glaucomatous eyes.[24] To evaluate the relationship between the VFs and the cpRNFLTs, several function–structure maps have been proposed. In these maps, a clustering of VF test points was performed.[14–18]

To cluster the VF test points, many investigators used factor analysis or cluster analysis.[10,11,13,15,19–23] Most of the factor analysis or cluster analysis studies used either the 30-2 or the 24-2 (Figs. 1A, 1B, respectively) or the 10-2 (Fig. 1C) VF test programs. Factor analyses were performed based on the

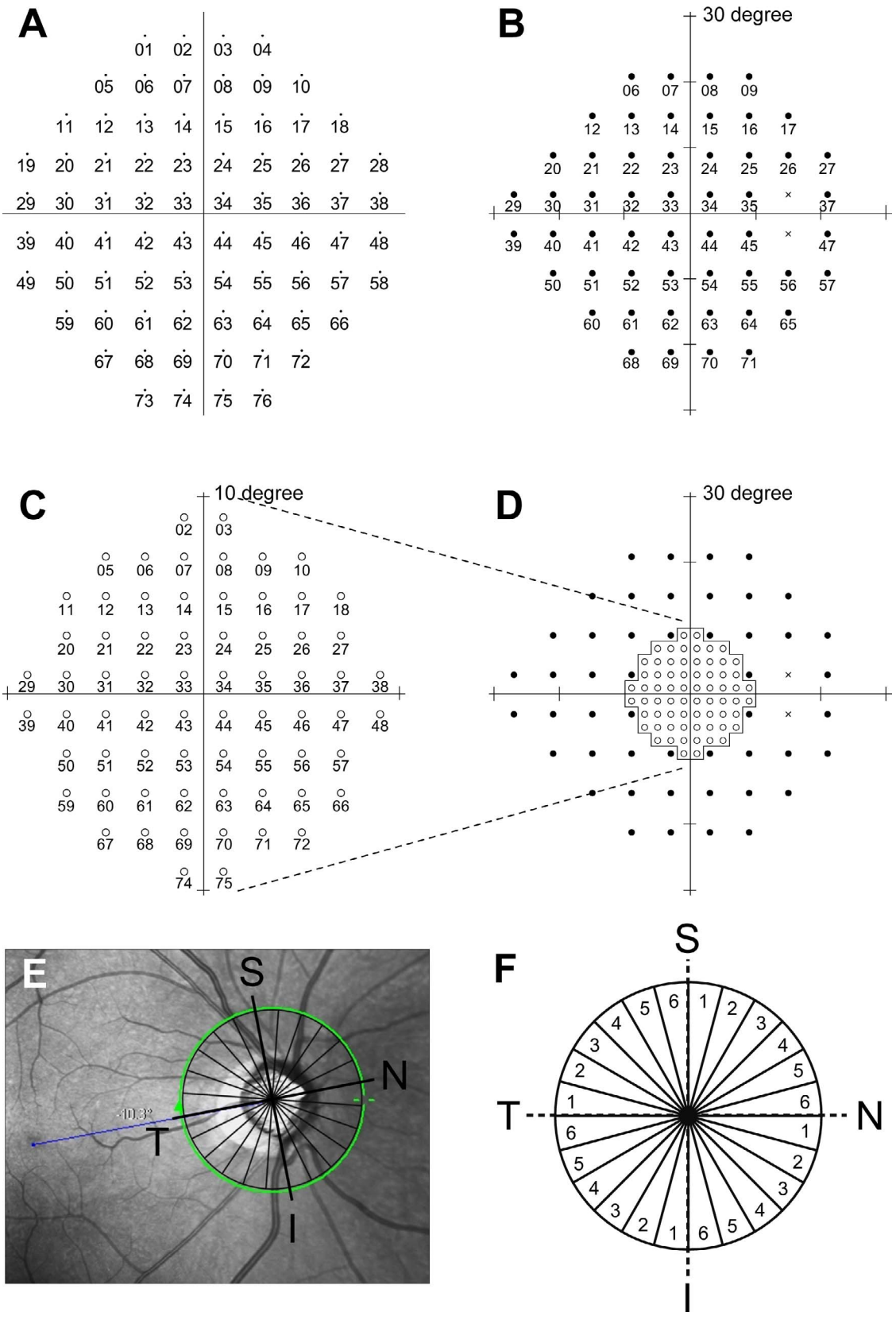

Figure 1. Visual field test grids and sectorization of circumpapillary SD-OCT scans of the right eye. The VF tests were performed with the HFA (Carl Zeiss Meditec), and the SD-OCT examinations were performed with the Spectralis OCT (Heidelberg Engineering). Left eye data were converted into right eye format for the analyses. (**A**) The HFA can test a maximum of 77 points (shown 76 points and 1 point corresponding with the fovea). We excluded the test point corresponding with the fovea from the analyses. (**B**) The 24-2 program examines 52 test points. (**C**) The 10-2 program tests 68 points. (**D**) The 24-2 and 10-2 VFs were combined as a single 24-2/10-2 VFs with 116 test points. Among the test points, the coordinates of the four parafoveal points in the 24-2 VFs overlapped the test points of 10-2 VFs. For these four overlapping points, the 10-2 VFs values were used to

make the combined VFs. (**E**, **F**) For the cpRNFLT evaluation, a 12°-diameter-circle B-scan centered on the ONH (i.e., a circumpapillary scan) was performed. The 768-point cpRNFLT values along the 360° scan were grouped into 24 sectors of 15° width. The reference axis of 0° to create the 24-sector cpRNFLT data was set as the line passing through the center of the fovea and the center of the circumpapillary SD-OCT scan (i.e., the fovea–ONH center axis).

intercorrelations of the variables[25]; thus, the results using a combined 24-2 and 10-2 VFs would have more information than the results using either the 24-2 VF or the 10-2 VF.

The purpose of this study was to group the 116 test points of the combined SITA-standard 24-2 and 10-2 VF test grids into a smaller number of VF clusters based on the latent factors found by explanatory factor analysis (EFA) to test the hypothesis that this method will demonstrate a detailed continuity of the 24-2 and 10-2 VF grids and finer distributions of the VF clusters for clinicians. We also performed EFA to group 24 sectors of the cpRNFLT to construct a smaller number of cpRNFL clusters. We then determined the correlations between the VF clusters and the cpRNFL clusters to test the hypothesis that these methods would optimize and strengthen the structure–function relationships.

Methods

The procedures used in this retrospective, cross-sectional, cohort study adhered to the tenets of the Declaration of Helsinki and were approved by the Institutional Review Board and Ethics Committee of Kyoto University Graduate School of Medicine.

Subjects

We reviewed the medical records of individuals who were seen by the Glaucoma Service at the Kyoto University Hospital between January 2012 and December 2014. The inclusion criteria were presence of both reliable 24-2 and 10-2 VF test (24-2 and 10-2 VFs) results obtained by SAP (HFA; Carl Zeiss Meditec). In addition, all of the eyes had undergone confocal scanning laser ophthalmoscopy (cSLO) and had SD-OCT examinations with the Spectralis SD-OCT (Heidelberg Engineering, Heidelberg, Germany) within a 3-month period. The axial lengths were measured by partial coherence interferometry (IOL Master; Carl Zeiss Meditec), and the axial length of all of the studied eyes was <27.0 mm. Eyes were excluded if a peripheral anterior synechia or appositional closure of the angle was detected by gonioscopy; if a prior or ongoing uveitis was present; corneal opacities, dense cataracts, or vitreous opacities were present; other ocular diseases such as retinal vein occlusion were present; and prior vitreoretinal or refractive surgery except for cataract surgery had been performed. In the end, a total of 254 eyes of 166 Japanese subjects were studied.

Visual Field Tests With Humphrey 24-2 and 10-2 Programs

Visual field tests were performed by standard automated perimetry (HFA; Carl Zeiss Meditec). The 24-2 and 10-2 VFs tests were performed under the same conditions (i.e., standard strategy with background illumination of 31.5 apostilb, stimulus size Goldmann III, stimulus color white, and SITA).[1,2] The VF results were considered reliable if they had a false-positive error rate of <33%, a false-negative error rate of <33%, and a fixation loss of <20%.

The 24-2 and 10-2 programs can obtain the threshold sensitivity, total deviation (TD), and pattern deviation (PD) values of 52 and 68 test points, respectively (Figs. 1B, 1C, respectively). There was a slight difference in the normative data between the SITA Standard 24-2 and the 10-2 that could have resulted in a slight difference of the TD and PD values despite the same threshold value in 24-2 and 10-2. Therefore, the threshold sensitivity values of each test point were used to combine the 24-2 and 10-2 test results. We excluded the threshold sensitivity value of the fovea from the analyses.

For the statistical analyses, the threshold sensitivity values on a decibel scale were converted to 1/Lambert (1/L) scale using the following formula[26]:

$$\mathrm{dB} = 10 \times \log_{10}(1/\mathrm{L}).$$

For the factor analyses, the 24-2 and 10-2 VFs were combined into a single 24-2/10-2 VF (Figs. 1B–D). Among the test points, the coordinates of four of the parafoveal points in the 24-2 VFs overlapped the test points of 10-2 VFs. For the overlapped four test points, the 10-2 VFs values were used to make the combined VFs. We excluded the test point corresponding with the fovea. Thus, the combined 24-2/10-2 VFs had 116 test points ($52 + 68 - 4 = 116$; Fig. 1D).

Circumpapillary RNFLT Evaluation Using Spectralis OCT

The studied eyes had undergone simultaneous cSLO and SD-OCT examinations using the Spectralis SD-OCT (Heidelberg Engineering) within 3 months of the VF tests.

For the cpRNFLT evaluations, a 12°-diameter-circle B-scan centered on the optic nerve head (ONH; circumpapillary scan) was obtained. Using the licensed software of "RNFL Export" (Heidelberg Engineering), 768 values of the RNFLT along the 360° OCT circle scan were obtained. The reference axis of 0° to create the 24-sector cpRNFLT data was set as a line that passed through the center of the fovea and the center of the SD-OCT circumpapillary scan (i.e., the fovea–ONH center axis; Fig. 1E). The angle between the fovea–ONH axis and the horizontal axis on the cSLO image was measured using the built-in software.

For the factor analyses, the 768 cpRNFLT values were combined into the same 15°-wide 24 sectors (Fig. 1F). The data of the left eye were converted into the right eye format.

Statistical Analyses

Explanatory factor analyses were performed to determine the latent factors of the 116 VF test points that could be grouped into a smaller number of clusters that fit the glaucomatous VF defect pattern of the combined 24-2/10-2 VF results. The EFA was based on the intercorrelation matrices for the threshold sensitivity (in 1/L scale) of the combined 116 VF test points. To check the sampling adequacy for the EFA, Kaiser-Meyer-Olkin's index (KMO, index for overall variables) and measurements of the sampling adequacy index for each individual variable (MSAi) were calculated.[27] The EFA was also performed in the same way using only the 52 test points of the 24-2 VF to compare the results.

The EFA was performed using the minimum residual technique with promax rotation because the variables did not satisfy the assumption of multivariate normal distribution. To determine the optimal number of latent factors, we used the Bayesian information criterion (BIC). When comparing BIC

Table 1. Demographics of the Study Subjects and Eyes

Parameter	Value
Subjects, no.	166
Age, y	58.9 ± 12.5
Sex	
Men	78
Women	88
Eyes, no.	**254**
RL	
Right	128
Left	126
CCT, μm	525.6 ± 33.3
Axial length, mm	24.89 ± 1.37
MD values, dB	
24-2 program	−9.06 ± 8.23
10-2 program	−9.54 ± 8.86
PSD values, dB	
24-2 program	8.12 ± 4.97
10-2 program	7.88 ± 5.50
Glaucoma stage*	
Normal	13
PPG	25
Early POAG	81
Moderate POAG	52
Advanced POAG	83
cpRNFLT, μm	68.0 ± 16.0
Fovea–ONH center angle, deg†	−6.98 ± 3.85

CCT, central corneal thickness; PPG, preperimetric glaucoma.

* The perimetric glaucoma stage was defined as follows: early, MD > −6 dB; moderate, −6 dB ≥ MD ≥ −12 dB; advanced, MD < −12 dB.

† The angle between the fovea–ONH center axis and the horizontal axis.

values for multiple models, smaller BIC values suggested a better fit model.

Explanatory factor analysis was performed in the same way to explore the factors that could group the 24 cpRNFL sectors into smaller number of clusters that fit the pattern of glaucomatous cpRNFL thinning.

To evaluate the function–structure relationship between the VF and the cpRNFLT clusters derived from the EFAs, the correlations between the average sensitivity of each VF cluster and the average RNFLT of each cpRNFLT cluster were evaluated using Pearson's correlation analysis. We developed a function–structure correlation map based on the largest Pearson's correlation coefficients for each cpRNFLT cluster with the VF clusters.

All continuous values are presented as the means ± SDs. The level of statistical significance was set at $P < 0.05$. The statistical analyses were performed using software R (https://cran.r-project.org/index.html). The EFA were performed using R package 'psych'.

Results

Characteristics of Eyes

The demographics of the 254 eyes of 166 subjects studied are shown in Table 1. The mean ± SD age of the 166 subjects was 58.9 ± 12.5 years. The mean axial length of the 254 eyes was 24.89 ± 1.37 mm. Among the 254 eyes, 13 eyes (5.1%) were diagnosed to be normal, 25 eyes (9.8%) as preperimetric primary open-angle glaucoma (POAG), and the other 216 eyes were diagnosed as perimetric POAG. Of the 216 perimetric glaucomatous eyes, 81 eyes (31.9%) had early glaucoma (MD for the 24-2 VF > −6 dB), 52 eyes (20.5%) had moderate glaucoma (−6 dB ≥ MD for the 24-2 VF ≥ −12 dB), and the other 83 eyes (32.7%) had advanced glaucoma (MD for the 24-2 VF < −12 dB). The mean degree of the fovea–ONH center axis was −6.98° ± 3.85°, with a range from −18.4° to +5.3° and a median of −7.3°.

The KMO index was 0.957 for the combined 116 VF test points and 0.829 for the 24 cpRNFLT sectors. The KMO and MSAi values ranged from 0.0 to 1.0, and usually a KMO >0.6 was accepted as a satisfactory factor analysis to proceed. Variables with MSAi <0.50 suggested that the item did not belong to the group and should be removed from the factor analysis.[27] All of the variables (i.e., 116 VF test points and 24 cpRNFL sectors) had MSAi values >0.75; thus, all of the variables were used for the EFAs.

Explanatory Factor Analyses in Combined 24-2 and 10-2 VF Test Results

The factor pattern matrix for the combined 116 VF test points is shown in Supplementary Table S1, which was created from the EFA using the minimum residual technique with promax rotation. The scree plot of the eigenvalues from the EFA is shown in Supplementary Figure S1A. The goodness-of-fit evaluation using the BIC values suggested that the optimal number of factors in the EFA for the 116 VF test points was 10. In this model, the accumulated percentage of common variance explained by the 10 common factors was 79.9%. By grouping the 116 VF test points based on the common factor with the largest factor loading, the EFA suggested that the VF test points could be grouped into nine VF clusters. Among them, the clusters based on factor 8 and factor 9 contained two discontinuous VF test points and only one VF test point, respectively (Fig. 2A). According to the second largest factor loading, each VF test point was grouped into cluster "VF-3" based on factor 3, cluster "VF-1" based on factor 1, and cluster "VF-4" based on factor 4 for clinical use and the following statistical analyses. Thus, the combined 116 VF test points were grouped into seven VF clusters based on the EFA (Fig. 2C).

Cluster VF-1 (red colored in Fig. 2C) included the superior nasal step and the parafoveal scotoma area, cluster VF-2 (blue colored in Fig. 2C) included the inferior parafoveal scotoma area, cluster VF-3 (light blue colored in Fig. 2C) included the superior midperipheral scotoma area, cluster VF-6 (green colored in Fig. 2C) included the inferior nasal step area, and cluster VF-7 (orange colored in Fig. 2C) included the inferior midperipheral scotoma area. Cluster VF-4 (pink colored in Fig. 2C) was overlapped in the superior and inferior hemifields and included the cecocentral scotoma area. Cluster VF-5 (yellow-green colored in Fig. 2C) included the superior cecocentral scotoma area of 24-2 VF test points.

For the EFA using only the 52 test points of the 24-2 VF, the suggested optimal number of factors was 7, and the accumulated percentage of common variance explained by the seven common factors was 76.3%. The EFA suggested that the 52 test points of the 24-2 VF could be grouped into six VF clusters (Supplementary Fig. S2A).

Explanatory Factor Analysis in 24-Sectored cpRNFLT

The factor pattern matrix for the 24 cpRNFLT sectors is shown in Supplementary Table S2. The scree plot of the eigenvalues

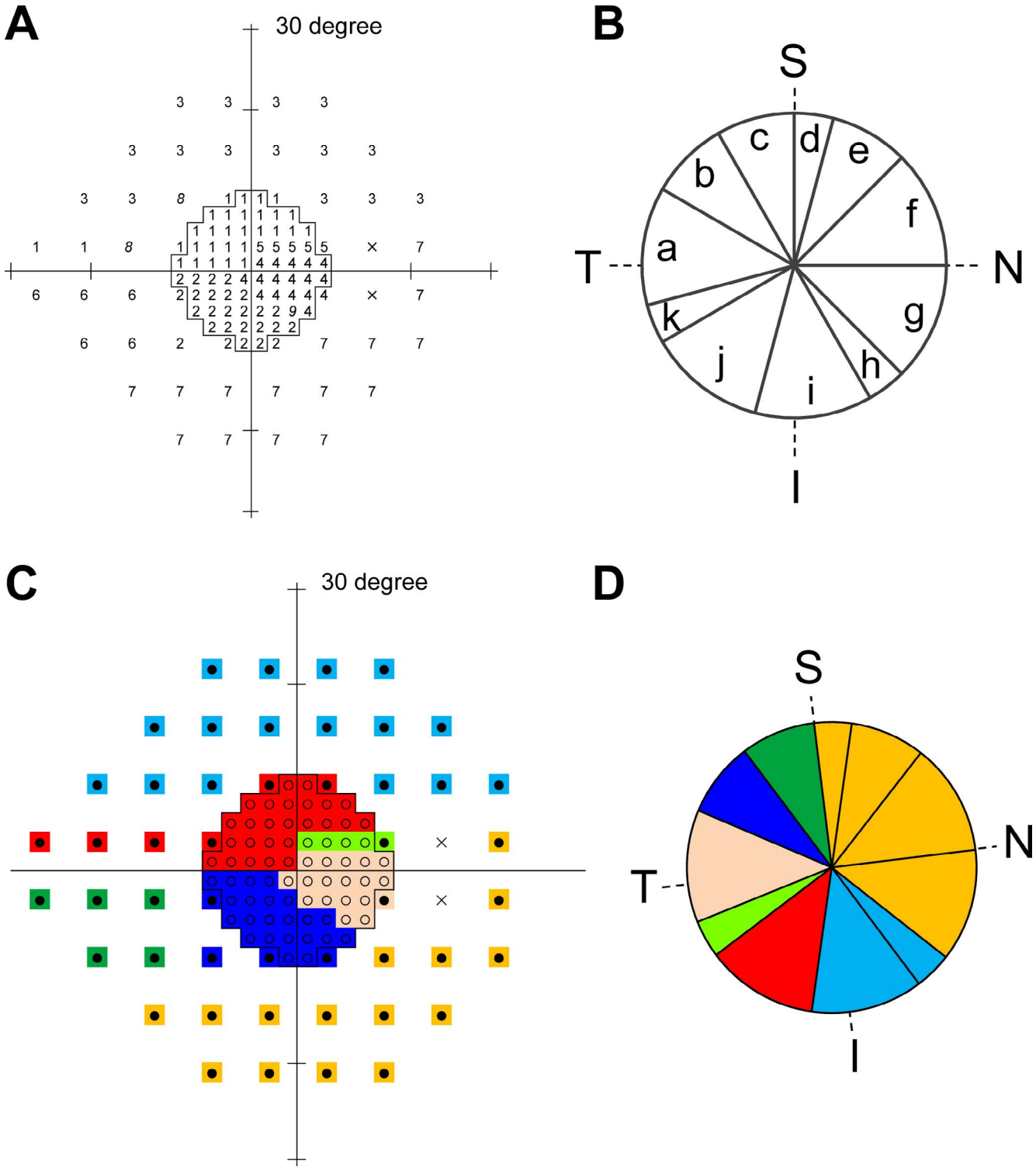

Figure 2. Clustering maps of VF test points and cpRNFLT sectors using EFA. The pattern matrix of the EFA for the combined 116 VF test points is shown in Supplementary Table S1, and the pattern matrix of the EFA for the 24 cpRNFLT sectors is shown in Supplementary Table S2. (**A**) Mapping of the factor numbers with the largest factor loadings of the 116 test points of combined 24-2 and 10-2 VF tests. By grouping the 116 VF test points based on the common factors with the largest factor loading, the EFA suggested that the VF test points could be grouped into nine VF clusters. Among them, clusters based on factor 8 and factor 9 contained two discontinuous VF test points and only one VF test point, respectively (shown in italics). According to the second largest factor loading, each VF test point was grouped into the cluster based on factors 3, 1, and 4, respectively (Supplementary Table S1). Finally, the combined 116 VF test points were grouped into seven VF clusters. (**B**) The EFA suggested that the 24 cpRNFLT sectors could be grouped into 11 clusters based on the common factor with the largest factor loading. (**C**, **D**) Color-coded maps showing the correlations between the VF test clusters and the cpRNFLT clusters. The correlation matrix of the 7 VF clusters and 11 cpRNFLT clusters is shown in Table 2. The mean degree of fovea–ONH center axis was –6.98° ± 3.85°.

Investigative Ophthalmology & Visual Science

Investigative Ophthalmology & Visual Science

TABLE 2. Pearson Correlation Matrix Between 7 VF Clusters and 11 cpRNFL Clusters

VF Cluster Name	VF Characteristics	cpRNFL Cluster Name (Clockwise Degree From the Fovea–ONH Center Axis*)										
		CP-a, −15 to 30	CP-b, 30–60	CP-c, 60–90	CP-d, 90–105	CP-e, 105–135	CP-f, 135–180	CP-g, 180–225	CP-h, 225–240	CP-i, 240–285	CP-j, 285–330	CP-k, 330–345
VF-03	Superior midperipheral scotoma	0.260	0.333	0.289	0.216	0.273	0.207	0.231	**0.334**	**0.624**	0.587	0.409
VF-01	Superior nasal step and parafoveal scotoma	0.294	0.356	0.376	0.255	0.229	0.181	0.190	0.316	0.550	**0.794**	0.564
VF-05	Superior cecocentral scotoma	0.436	0.403	0.343	0.175	0.171	0.094	0.119	0.235	0.433	0.597	**0.725**
VF-04	Cecocentral scotoma overlapped in the superior and inferior hemifields	**0.637**	0.582	0.415	0.307	0.309	0.228	0.230	0.224	0.365	0.365	0.539
VF-02	Inferior parafoveal scotoma	0.486	**0.766**	0.639	0.445	0.395	0.289	0.250	0.233	0.383	0.349	0.376
VF-06	Inferior nasal step	0.322	0.652	**0.719**	0.456	0.367	0.282	0.215	0.188	0.380	0.365	0.288
VF-07	Inferior midperipheral scotoma	0.311	0.574	0.622	**0.477**	**0.541**	**0.384**	**0.304**	0.301	0.416	0.266	0.267

The position of the VF and cpRNFL clusters are shown in Figures 2A, 2B. The largest Pearson's correlation coefficient in each column is shown in bold. CP, circumpapillary.
* The reference of the clockwise degrees in the cpRNFLT sector was set as the fovea–optic nerve head center axis (shown in Fig. 1E).

from the EFA is shown in Supplementary Figure S1B. The goodness-of-fit evaluations using the BIC values suggested that the optimal number of factors in the EFA for the 24 sector cpRNFLT was 11. In this model, the accumulated percentage of common variance explained by the 11 common factors was 84.2%. By grouping the 24 cpRNFLT sectors with the largest factor loadings, the EFA indicated that the cpRNFLT sectors could be grouped into 11 clusters (Fig. 2B).

Correlation Between VF Clusters and cpRNFLT Clusters

Pearson's correlation coefficient between the average sensitivity of the combined 116 VF test points and the average cpRNFLT was better when using the average sensitivity of the 1/L scale ($r = 0.743$, 95% confidence interval [CI] = 0.683–0.794) than when using the average sensitivity of the decibel scale ($r = 0.719$, 95% CI = 0.654–0.774). Thus, the correlations between the average sensitivity of each VF cluster in the 1/L scale and the average RNFLT in each cpRNFLT cluster in micrometers were used to evaluate the function–structure relationship between the VF and the cpRNFLT clusters both derived from the EFAs.

Pearson's correlation matrix between the average sensitivities of the 7 VF clusters and the average RNFLT of the11 cpRNFL clusters is shown in Table 2. Based on the highest correlation coefficients, a new function–structure relationship map was developed (Figs. 2C, 2D). The correlation coefficients between the corresponding VF and cpRNFLT clusters ranged from 0.304 to 0.794 (Table 2).

DISCUSSION

Our EFA using the 116 test points of the combined 24-2 and 10-2 VFs found seven VF clusters that fit the pattern of glaucomatous VF defects. Another EFA was performed on the 24-sectored cpRNFLT that found cpRNFLT clusters that fit the pattern of glaucomatous cpRNFL thinning. In the studied eyes, the average sensitivity of the combined 116 VF test points in the decibel scale had a curvilinear relationship to the cpRNFLT and had a better fit to the linear relationship after converting to 1/L scale. Thus, the average sensitivity of each VF cluster in the 1/L scale was used to evaluate the function–structure relationship. The EFAs were performed independently, and the average threshold sensitivity in the 1/L scale and cpRNFLT in the corresponding clusters were moderately to highly correlated. These results indicate that the pattern of glaucomatous VF defect and cpRNFLT thinning had common latent factors that might be derived from a developing pattern of glaucomatous optic neuropathy. These findings support the function–structure relationship theory in glaucoma.[28–30]

Based on the correlation between the VF clusters and cpRNFLT clusters both derived from the EFAs independently, we were able to develop a new function–structure relationship map. A few earlier studies showed their function–structure relationship map, and three different methods were used to evaluate the relationship between the SAP VF test grid and cpRNFLT. Garway-Heath et al.[14] and Hood et al.[18] projected the 24-2 or 10-2 VF test grid onto fundus photographs or OCT retinal thickness maps. Kanamori et al.[16] calculated the correlation between the TD values of each 24-2 VF test point and the RNFLT of each cpRNFL sector. These studies used different approaches from that used in this study. Ferreras et al.[15] grouped the 24-2 VF test points using EFA and then evaluated the correlation between each VF cluster and 12-sectored cpRNFLT.

Our study also used EFAs, but we combined the 24-2 and 10-2 VF test results and also performed EFA to group 24 sectored cpRNFLTs into 11 cpRNFLT clusters before evaluation of function–structure correlation. Our results indicated higher correlation coefficients than the earlier study,[15] and this suggests that our approach could optimize the strength of function–structure relationships. In addition, our results did not rule out the function–structure correlation in the other clusters where Pearson's coefficients were lower.

We used both the 24-2 and 10-2 VF tests and grouped the combined 116 test points using EFA. In earlier studies, investigators used factor analysis or cluster analysis to group the VF test points.[10,11,13,15,19–23] However, most of the studies used either the 30-2/24-2 or the 10-2 VF tests only. Factor analysis is performed based on the intercorrelation of variables; thus, the results using 116 test points of combined 24-2 and 10-2 VFs should have more information than the results using the 52 test points of 24-2 VF or the 68 test points of 10-2 VF only. Indeed, we could identify four clusters that overlapped in the 24-2 and 10-2 VF grids. These detailed continuity and fine distributions of the clusters could not be identified if the EFA was performed using 24-2 VF only (Supplementary Fig. S2). The results showed the relationships between the finer VF clusters and cpRNFLT as a function–structure relationship map. These results showed how clinicians should compare function and structure information when 24-2 and 10-2 VF results are available at the same time.

The VF tests in this study were performed using the SITA. The SITA strategy was developed to be similarly accurate with reducing test time compared with the Full Threshold algorithm.[1,2] This algorithm has information about the correlations between the threshold sensitivities at different test points and deduces the sensitivity of certain test points from the sensitivity of other test points. Thus, the VF clusters obtained in this study might be attributable to the strategy used (i.e., the SITA standard). The SITA was designed to facilitate work in routine clinical practice and has become the clinical standard for both the diagnosis and management of glaucoma. The results of our study provide clinicians detailed VF clusters and new information about function–structure relationship, but the strategy used needs to be considered in interpreting the findings.

The VF clusters in the superior and inferior hemifields were asymmetrical, and the horizontally asymmetrical cluster VF-4 (pink colored in Fig. 2C) was between fixation and the optic disc (i.e., the cecocentral area, which consisted of the less vulnerable macular region proposed by Hood et al.).[31] On the other hand, the position of the cpRNFLT cluster corresponding to the VF-4 cluster (cluster CP-a; pink colored in Fig. 2D) was slightly different from that of an earlier study.[31] The reason for the difference in the position of the corresponding cpRNFLT cluster might be the difference in the reference axis of the cpRNFLT. The reference of the clockwise degrees in the cpRNFLT sector was set as the horizontal axis of the fundus image in the studies of Hood et al.,[31] whereas it was set as the fovea–ONH center axis in this study. The fovea is usually located below the ONH center in fundus images, and the degree varies among individuals.[14,32] We set the reference line as the fovea–ONH center axis to minimize the influence of the variability, although the effect was not fully determined.[33–36]

The 24-2 VF grid has four test points between (and including) fixation and the optic disc (i.e., test point numbers 34, 35, 44, and 45 in Fig. 1B). However, the cecocentral scotoma cluster VF-4 (pink colored in Fig. 2C) included only two of the four test points in the 24-2 VF (i.e., inferior test points number 44 and 45 in Fig. 1B). The superior hemifield of the VF-4 cluster could be evaluated using 10-2 VF, but could be overlooked when using only 24-2 VF. Therefore, if the 24-2 VF results show a deep depression in the threshold sensitivities in the inferior cecocentral test points, additional use of 10-2 VFs would be strongly recommended to evaluate a cecocentral scotoma more carefully.

There are several limitations in this study. First, this was a cross-sectional retrospective study includes a selection bias. The studied eyes had undergone the 24-2 VF test, 10-2 VF test, and cpRNFLT evaluation using SD-OCT within a 3-month period. The individuals seen in our Glaucoma Service do not routinely undergo these examinations in this schedule. The studied eyes were suspected of having paracentral or cecocentral scotoma and thus had undergone these examinations within the 3-month period. In results, the mean MD examined with the 10-2 program (–9.54 ± 8.86 dB) was equal or worse than that obtained with the 24-2 program (–9.06 ± 8.23 dB). Second, the sample size of 254 eyes was small relative to the number of 116 VF test points, and both eyes were included for the analyses in more than one half of the subjects. This method could increase sample size to raise the statistical power, but the common factors between the two eyes could cause inflations of the intercorrelation of the variables. Third, eyes with relatively longer axial length (<27 mm) were also included to increase sample size. Both the SAP sensitivity and cpRNFLT could have been influenced by the high myopia.[37–39] Finally, this cross-sectional retrospective study could not evaluate the intersession variability of each VF or cpRNFLT cluster values. To overcome these limitations, future prospective studies with larger sample sizes and strict inclusion criteria are needed.

In conclusion, we grouped the 116 test points of the combined 24-2 and 10-2 VF test grid into seven VF clusters based on the latent factors found by EFA. We performed another EFA that resulted in grouping the 24 sectors of circumpapillary SD-OCT scans into 11 cpRNFLT clusters. The average threshold sensitivity and the average cpRNFLT in the corresponding clusters were moderately to highly correlated. Our results indicate that the pattern of glaucomatous VF defect and cpRNFLT thinning had common latent factors that support the function–structure relationship theory in glaucoma.

Acknowledgments

Supported by the Innovative Techno-Hub for Integrated Medical Bio-Imaging of the Project for Developing Innovation Systems from the Ministry of Education, Culture, Sports, Science and Technology, Japan.

Disclosure: **H. Nakanishi**, None; **T. Akagi**, None; **K. Suda**, None; **T. Hasegawa**, None; **H. Yamada**, None; **S. Yokota**, None; **M. Yoshikawa**, None; **Y. Iida**, None; **H.O. Ikeda**, None; **S. Morooka**, None; **K. Ishihara**, None; **N. Yoshimura**, None

References

1. Bengtsson B, Olsson J, Heijl A, Rootzén H. A new generation of algorithms for computerized threshold perimetry, SITA. *Acta Ophthalmol Scand*. 1997;75:368–375.
2. Bengtsson B, Heijl A. Evaluation of a new perimetric threshold strategy, SITA, in patients with manifest and suspect glaucoma. *Acta Ophthalmol Scand*. 1998;76:268–272.
3. Flammer J, Drance S, Zulauf M. Differential light threshold. Short- and long-term fluctuation in patients with glaucoma, normal controls, and patients with suspected glaucoma. *Arch Ophthalmol*. 1984;102:704–706.
4. Heijl A, Lindgren A, Lindgren G. Test-retest variability in glaucomatous visual fields. *Am J Ophthalmol*. 1989;108:130–135.
5. Chauhan BC, Garway-Heath DF, Goni FJ, et al. Practical recommendations for measuring rates of visual field change in glaucoma. *Br J Ophthalmol*. 2008;92:569–573.

6. Wirtschafter JD, Becker WL, Howe JB, Younge BR. Glaucoma visual field analysis by computed profile of nerve fiber function in optic disc sectors. *Ophthalmology*. 1982;89:255–267.
7. Werner EB, Bishop KI, Koelle J, et al. A comparison of experienced clinical observers and statistical tests in detection of progressive visual field loss in glaucoma using automated perimetry. *Arch Ophthalmol*. 1988;106:619–623.
8. Katz J, Sommer A, Gaasterland DE, Anderson DR. Comparison of analytic algorithms for detecting glaucomatous visual field loss. *Arch Ophthalmol*. 1991;109:1684–1689.
9. Weber J, Ulrich H. A perimetric nerve fiber bundle map. *Int Ophthalmol*. 1991;15:193–200.
10. Mandava S, Zulauf M, Zeyen T, Caprioli J. An evaluation of clusters in the glaucomatous visual field. *Am J Ophthalmol*. 1993;116:684–691.
11. Suzuki Y, Araie M, Ohashi Y. Sectorization of the central 30 degrees visual field in glaucoma. *Ophthalmology*. 1993;100:69–75.
12. Asman P, Heijl A. Arcuate cluster analysis in glaucoma perimetry. *J Glaucoma*. 1993;2:13–20.
13. Koseki N, Araie M, Yamagami J, Suzuki Y. Sectorization of central 10-deg visual field in open-angle glaucoma—an approach for its brief evaluation. *Graefe's Arch Clin Exp Ophthalmol*. 1995;233:621–626.
14. Garway-Heath DF, Poinoosawmy D, Fitzke FW, Hitchings RA. Mapping the visual field to the optic disc in normal tension glaucoma eyes. *Ophthalmology*. 2000;107:1809–1815.
15. Ferreras A, Pablo LE, Garway-Heath DF, Fogagnolo P, García-Feijoo J. Mapping standard automated perimetry to the peripapillary retinal nerve fiber layer in glaucoma. *Invest Ophthalmol Vis Sci*. 2008;49:3018–3025.
16. Kanamori A, Naka M, Nagai-Kusuhara A, Yamada Y, Nakamura M, Negi A. Regional relationship between retinal nerve fiber layer thickness and corresponding visual field sensitivity in glaucomatous eyes. *Arch Ophthalmol*. 2008;126:1500–1506.
17. Asaoka R, Russell RA, Malik R, Crabb DP, Garway-Heath DF. A novel distribution of visual field test points to improve the correlation between structure-function measurements. *Invest Ophthalmol Vis Sci*. 2012;53:8396–8404.
18. Hood DC, Raza AS, de Moraes CGV, Johnson CA, Liebmann JM, Ritch R. The nature of macular damage in glaucoma as revealed by averaging optical coherence tomography data. *Trans Vis Sci Tech*. 2012;1(1):3.
19. Nouri-Mahdavi K, Mock D, Hosseini H, et al. Pointwise rates of visual field progression cluster according to retinal nerve fiber layer bundles. *Invest Ophthalmol Vis Sci*. 2012;53:2390–2394.
20. Asaoka R. Mapping glaucoma patients' 30-2 and 10-2 visual fields reveals clusters of test points damaged in the 10-2 grid that are not sampled in the sparse 30-2 grid. *PLoS One*. 2014;9:6–11.
21. De Moraes CG, Song C, Liebmann JM, Simonson JL, Furlanetto RL, Ritch R. Defining 10-2 visual field progression criteria: Exploratory and confirmatory factor analysis using pointwise linear regression. *Ophthalmology*. 2014;121:741–749.
22. Hirasawa K, Murata H, Hirasawa H, Mayama C, Asaoka R. Clustering visual field test points based on rates of progression to improve the prediction of future damage. *Invest Ophthalmol Vis Sci*. 2014;55:7681–7685.
23. Suzuki Y, Kitazawa Y, Araie M, et al. Mathematical and optimal clustering of test points of the central 30-degree visual field of glaucoma. *J Glaucoma*. 2001;10:121–128.
24. Sung KR, Kim JS, Wollstein G, Folio L, Kook MS, Schuman JS. Imaging of the retinal nerve fibre layer with spectral domain optical coherence tomography for glaucoma diagnosis. *Br J Ophthalmol*. 2011;95:909–914.
25. Gorsuch RL. *Factor Analysis*. 2nd Ed. Hillsdale, NJ: Lawrence Erlbaum Associates, Inc.; 1983.
26. Garway-Heath DF, Caprioli J, Fitzke FW, et al. Scaling the hill of vision: the physiological relationship between light sensitivity and ganglion cell numbers. *Invest Ophthalmol Vis Sci*. 2000;41:1774–1782.
27. Kaiser H, Rice J. Little jiffy, mark iv. *Educ Psychol Meas*. 1974;34:111–117.
28. Harwerth RS, Wheat JL, Fredette MJ, Anderson DR. Linking structure and function in glaucoma. *Prog Retin Eye Res*. 2010;29:249–271.
29. Hood DC, Kardon RH. A framework for comparing structural and functional measures of glaucomatous damage. *Prog Retin Eye Res*. 2007;26:688–710.
30. Sharma P, Sample PA, Zangwill LM, Schuman JS. Diagnostic tools for glaucoma detection and management. *Surv Ophthalmol*. 2008;53:S17–S32.
31. Hood DC, Nguyen M, Ehrlich AC, et al. A test of a model of glaucomatous damage of the macula with high-density perimetry: implications for the locations of visual field test points. *Trans Vis Sci Tech*. 2014;3(3):5.
32. Chauhan BC, O'Leary N. Almobarak FA, et al. Enhanced detection of open-angle glaucoma with an anatomically accurate optical coherence tomography-derived neuroretinal rim parameter. *Ophthalmology*. 2013;120:535–543.
33. Amini N, Nowroozizadeh S, Cirineo N, et al. Influence of the disc-fovea angle on limits of RNFL variability and glaucoma discrimination. *Invest Ophthalmol Vis Sci*. 2014;55:7332–7342.
34. Resch H, Pereira I, Hienert J, et al. Influence of disc-fovea angle and retinal blood vessels on interindividual variability of circumpapillary retinal nerve fibre layer. *Br J Ophthalmol*. 2016;100:531–536.
35. Danthurebandara VM, Sharpe GP, Hutchison DM, et al. Enhanced structure-function relationship in glaucoma with an anatomically and geometrically accurate neuroretinal rim measurement. *Invest Ophthalmol Vis Sci*. 2014;56:98–105.
36. Choi JA, Kim JS, Park HY, Park H, Park CK. The foveal position relative to the optic disc and the retinal nerve fiber layer thickness profile in myopia. *Invest Ophthalmol Vis Sci*. 2014;55:1419–1426.
37. Aung T, Foster PJ, Seah SK, et al. Automated static perimetry: the influence of myopia and its method of correction. *Ophthalmology*. 2001;108:290–295.
38. Kang SH, Hong SW, Im SK, Lee SH, Ahn MD. Effect of myopia on the thickness of the retinal nerve fiber layer measured by Cirrus HD optical coherence tomography. *Invest Ophthalmol Vis Sci*. 2010;51:4075–4083.
39. Oner V, Aykut V, Tas M, Alakus MF, Iscan Y. Effect of refractive status on peripapillary retinal nerve fibre layer thickness: a study by RTVue spectral domain optical coherence tomography. *Br J Ophthalmol*. 2013;97:75–79.

Investigative Ophthalmology & Visual Science